Backward correlations and dynamic heterogeneities: a computer study of ion dynamics

A. Heuer,* M. Kunow,† M. Vogel,‡ and R.D. Banhatti§
Westfälische Wilhelms-Universität Münster
Institut für Physikalische Chemie and Sonderforschungsbereich 458
Schlossplatz 4/7, D-48149 Münster, Germany
(Dated: February 1, 2008)

We analyse the correlated back and forth dynamics and dynamic heterogeneities, i.e. the presence of fast and slow ions, for a lithium metasilicate system via computer simulations. For this purpose we define, in analogy to previous work in the field of glass transition, appropriate three-time correlation functions. They contain information about the dynamics during two successive time intervals. First we apply them to simple model systems in order to clarify their information content. Afterwards we use this formalism to analyse the lithium trajectories. A strong back-dragging effect is observed, which also fulfills the time-temperature superposition principle. Furthermore, it turns out that the back-dragging effect is long-ranged and exceeds the nearest neighbor position. In contrast, the strength of the dynamic heterogeneities does not fulfill the time-temperature superposition principle. The lower the temperature, the stronger the mobility difference between fast and slow ions. The results are then compared with the simple model systems considered here as well as with some lattice models of ion dynamics.

PACS numbers: 66.30.Dn

I. INTRODUCTION

One basic characteristics of amorphous ion conductors is the strong frequency dependence of the conductivity at sufficiently low temperatures [1, 2, 3, 4]. According to linear response theory, the dispersion in $\sigma(\nu)$ is equivalent to a non-diffusive mean square displacement $\langle r^2(t)\rangle$ and thus to the presence of correlated back and forth jumps [1]. Neglecting possible dynamic correlations among adjacent ions the relation between both quantities reads

$$\sigma(\nu) = \frac{q^2\rho}{6k_BT}\int_0^\infty dt\,(d/dt)w(t)\exp(-i2\pi\nu t) \quad (1)$$

where q denotes the charge and ρ the density of the mobile ions. The function $w(t)$ is defined as

$$w(t) = (d/dt)\langle r^2(t)\rangle. \quad (2)$$

For very high frequencies one observes local dynamics which is strongly system-dependent. For example, in a sodium silicate system [5] one observes for $\nu < 10^{11}$ Hz a continuous decrease of $\sigma(\nu)$ with decreasing ν which can typically be attributed to non-local dynamics [6] and becomes stronger for decreasing temperature. Actually, this conclusion has been explicitly verified in recent simulations for lithium metasilicate [7]. In a double-logarithmic representation at low temperatures the apparent exponent decreases from one to zero until the d.c. plateau is reached, i.e. $\sigma(\nu) = \sigma_{d.c.}$.

In general, the complexity of ion dynamics in disordered systems is, on the one hand, related to the static disorder of the material and, on the other hand, to the Coulomb interaction among the ions giving rise to dynamic disorder. Therefore, one might expect that both the static as well as the dynamic disorder enhances the number of correlated back and forth jumps (see, however, Ref.[8]) although in recent simulations of sodium silicate at $T = 2000$ K no such correlations have been observed [9]. Furthermore, the presence of different environments of the network might imply that at a given time some ions are more mobile than other ions, i.e. there exist dynamic heterogeneities. Unfortunately, no direct information about dynamic heterogeneities can be gained from conductivity experiments or, equivalently, from the time dependence of the mean square displacement. Some progress has been achieved on the basis of simulations. Comparing the mean square displacement of different ions during a given time a broad distribution has been observed [10]. This basically corresponds to the presence of a large non-gaussian parameter which is known to represent dynamic heterogeneities quite well [11]. Other groups found an interesting spatial structure of the mobile regions [12, 13].

Another system with intrinsic complex dynamics is a glass-forming liquid. A tagged particle in a glass-former experiences a dramatic slowing down with decreasing temperature [14]. To a large extent this is related to the cage effect since at low temperatures the neighbour particles have a strong confining effect on the central particle [15]. This gives rise to strongly subdiffusive dynamics, i.e. to correlated back and forth dynamics. Furthermore glass-forming systems display dynamic heterogeneities [16, 17, 18, 19]. This property has been quantified by invoking appropriate three-time correlation func-

*Electronic address: andheuer@uni-muenster.de
†Electronic address: kunow@uni-muenster.de
‡Electronic address: mivogel@uni-muenster.de
§Electronic address: banhatt@uni-muenster.de

tions, containing information about the dynamics during two subsequent time intervals [20, 21, 22].

Using these three-time correlation functions one can hope to answer several basic questions about the complexity of ion dynamics. How relevant are backward correlations? Are back and forth correlations restricted to nearest-neighbor ionic positions? How does the tendency of these back and forth correlations depend on the time scale of investigation? Do dynamic heterogeneities depend on temperature and thus invalidate the time-temperature superposition principle, observed for many other quantities like the conductivity? This and other aspects of ionic dynamics will be analysed in this paper by invoking appropriate three-time correlation functions. They will be applied to computer generated trajectories of lithium metasilicate (Li_2O)(SiO_2). Very recently, first measurements of three-time correlations have been conducted via multidimensional NMR. These results clearly showed that dynamic heterogeneities are omnipresent in disordered ionic conductors [23]

The organization of this paper is as follows. In Section 2 we describe the technical aspects of the simulation and discuss the numerical tools. Section 3 introduces the concept of three-time correlations. Section 4 contains the analysis of simple model systems for which we clarify the information content of the three-time correlation functions. The results of our simulations as well as their interpretation are presented in Section 5. We close with a discussion and a summary in Section 6.

II. SIMULATION

The potential energy for the lithium silicate system is chosen to be the sum of a Buckingham and a Coulomb pair potential (i, j denote the species lithium, oxygen, or silicon, respectively)

$$U_{ij}(r) = \frac{q_i q_j e^2}{r} - \frac{C_{ij}}{r^6} + A_{ij} \exp(-B_{ij} r). \qquad (3)$$

The parameters have been determined by Habasaki et al. [24, 25]. Details of our simulation can be found in [7, 26]. Summarizing, we performed molecular dynamics simulations with a time step of 2 fs and a density of $\rho = 2.34$ g cm^{-3}. Periodic boundary conditions were used. The system size is 1152 particles, thus containing 384 lithium ions. The trajectories were generated by an appropriately modified version of the MOLDY software package, supplied by K. Refson [27]. The length of the production runs was 16 ns after an equilibration time of ca. 10 ns at the two lowest temperatures. Even at $T =$ 640 K the mean square displacement during the production time was larger than 60 Å^2 (nearest-neighbour Li-Li distance 2.6 Å); see Ref. [7]. All configurations were equilibrated at T = 1500 K. The computer glass transition is approximately 1100 K [7, 26]. In this work we present simulations for five temperatures (T = 1240 K, T = 980 K, 750 K, 700 K, and 640 K). For all temperatures, the lithium subsystem has been equilibrated before starting the production run. In particular at the lower temperatures the network fluctuations are very small (mean square displacement of 0.3 Å^2).

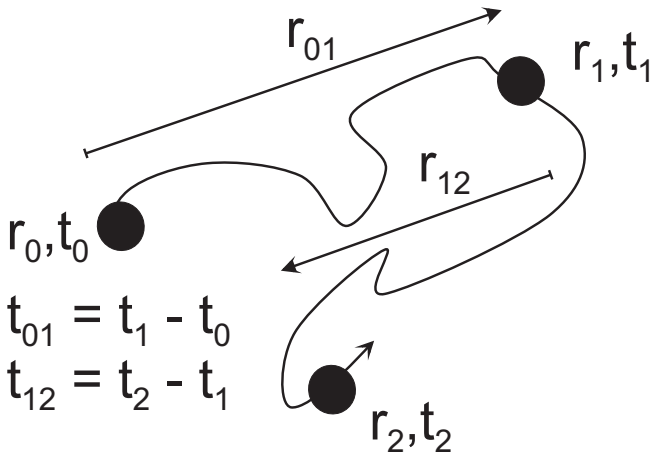

Figure 1: Sketch of a single-particle dynamics in order to clarify the definition of r_{01} and r_{12}.

III. THREE-TIME CORRELATIONS

A. Definition of three-time correlations

As mentioned above, the dispersive behavior of the conductivity or, equivalently, the non-diffusive behavior of the mean square displacement, has been related to correlated back and forth dynamics. Here we want to introduce a formalism which allows one to elucidate the properties of back and forth dynamics in detail. We remind the reader that standard observables for the characterization of dynamical properties like the mean square displacement correlate the position of individual ions at two successive times t_0 and t_1. For a calculation of $\langle r^2(t) \rangle$ one averages over the configurations at all times t_0 and t_1 such that $t_1 - t_0 = t$. Back and forth dynamics, however, is related to the properties of particles during two subsequent time intervals. Formally, this can be described as a three-time correlation, including a third time $t_2 > t_1$. The idea is sketched in Fig. 1. r_{01} denotes the distance a particle moves during the first time interval of length $t_{01} = t_1 - t_0$. The value of r_{12} denotes the motion during the second time interval of length $t_{12} = t_2 - t_1$ as projected on the direction of the motion during the first time interval. In case of a backjump, as shown for the example in Fig. 1, the value of r_{12} is counted negative. The additional information about the dynamics during two successive time intervals as compared to the dynamics during a single time interval is contained in the conditional probability function $p(r_{12}|r_{01})$ which denotes the probability for a specific value of r_{12} under the condition that the particle has moved the distance r_{01} in the first

time interval.

B. Moments

Rather than analysing the full probability function, we concentrate on the first moment $\bar{r}(r_{01})$ and the second moment $v(r_{01}) \equiv \langle (r_{12} - \bar{r}(r_{01}))^2 (r_{01}) \rangle$. The interpretation of both functions is straightforward. $\bar{r}(r_{01})$ contains information about the relevance of back and forth dynamics. In case that the direction of the dynamics during two successive time intervals is uncorrelated one expects $\bar{r}(r_{01}) = 0$. In contrast, a negative value of $\bar{r}$ is direct evidence of the presence of back and forth dynamics.

The second moment $v(r_{01})$ yields information about the presence of dynamic heterogeneities. In case that all particles have the same mobility, the distance moved in the second time interval is independent of the distance moved in the first time interval. Thus $v(r_{01})$ would *not* depend on r_{01}. A dependence on r_{01} will be observed if there exist fast and slow ions. The subensemble of ions with small r_{01} will preferably contain slow ions whereas for ions with large r_{01} it is vice versa. Therefore, ions with small r_{01} will on average move less in the second time interval t_{12} than ions with large r_{01}, resulting in a monotonous increase of $v(r_{01})$ with r_{01}.

C. First moment in the limit $t_{01} \to 0$

It is possible to establish a direct relation between the mean square displacement and the first moment $\bar{r}(r_{01})$ for the case of a discrete hopping model in the limit $t_{01} \to 0$. For reasons of simplicity we take a 1D model with distances d_0 between the individual sites. One may start with the simple relation

$$\langle r^2(t_{01}+t_{12}) \rangle = \langle r^2(t_{01}) \rangle + 2\langle r(t_{01}) r(t_{12}) \rangle + \langle r^2(t_{12}) \rangle \quad (4)$$

which is valid for stationary processes. On the left side one can perform a linear expansion around $t_{01} = 0$. On the right side one may use the fact that for very small t_{01} the term $\langle r^2(t_{01}) \rangle$ can be written as $\Gamma_{eff} d_0^2 t_{01}$ (corresponding to the short-time diffusion in pure hopping models with an effective escape rate Γ_{eff}). Since for very short times the system can only jump to the nearest neighbor site the term $\langle r(t_{01}) r(t_{12}) \rangle$ can be expressed as $\Gamma_{eff} d_0 t_{01} \bar{r}(d_0)$. Inserting these relations into Eq.4 one finally ends up with

$$\frac{\bar{r}(d_0)}{d_0} = \frac{1}{2} \left[\frac{w(t_{12})}{w(0)} - 1 \right]. \quad (5)$$

This relation directly shows that exactly in case of diffusive dynamics, i.e. $w(t) = const$, one has $\bar{r}(d_0) = 0$, i.e. no correlated back and forth dynamics. For subdiffusive behavior one obtains (beyond a possible oscillatory regime of the mean square displacement) $0 < w(t) < w(0)$ and thus $-1/2 < \bar{r}(d_0)/d_0 < 0$. Thus subdiffusive behavior is equivalent to the presence of correlated forward and backward jumps. Furthermore validity of Eq.5 implies that the first moment $\bar{r}(d_0)$ has a lower limit $-(1/2)d_0$ which is reached if $w(t) = 0$, i.e. for the long-time limit of localized dynamics where any forth jump is followed by a back jump . Finally one can see that the range of dispersion, i.e. $w(t \to \infty)/w(0)$, can be related to the first moment $\bar{r}(d_0)$ in the limit $t_{01} \to 0$ and $t_{12} \to \infty$.

This formal treatment has been performed for a hopping model with discrete sites. This may be considered as an appropriate model also for more realistic systems for which the particles will fluctuate around the individual sites. In particular this is the case for the ion conductor, studied in this work (see below for more details). In contrast, for glass-forming systems hopping dynamics is not so relevant. Therefore it is not possible to formulate such a simple relation between the derivative $w(t)$ of the mean square displacement and the first moment $\bar{r}(d_0)$.

Eq.5 also implies that the first moment $\bar{r}(d_0)$ in the limit $t_{01} \to 0$ does *not* contain new information as compared to the mean square displacement. For finite t_{01}, however, the first moment can no longer be predicted from $w(t)$. Thus new information as compared to the mean square displacement about the nature of correlated back and forth dynamics becomes available. Of particular interest is the dependence of the first moment on r_{01}. For example one can learn whether there exists a long-range back-dragging effect, as implied e.g. in the percolation approach of ion dynamics, or whether after jumping to the next nearest neighbor site the memory about the initial site has been basically wiped out.

IV. MODEL CALCULATIONS

In order to clarify the information content of the first moment $\bar{r}(r_{01})$ and the second moment $v(r_{01})$ we first calculate them for some simple one-dimensional models. We always consider the case of stochastic dynamics since we are interested in time scales which are beyond the ballistic regime.

A. Harmonic oscillator

This model is relevant to describe the backward and forward dynamics in the individual potential wells. We consider a harmonic oscillator with minimum at $r = 0$. Both times t_{01}, t_{12} are longer than the equilibration time of the oscillator, i.e. the mean square displacement is already constant. We first calculate the probability $p_1(r_1)$ that after the first time interval the system is at r_1 after a motion of r_{01} to the right. This can be formally calculated as

$$p_1(r_1) = \int_0^\infty dr_0 \, p_0(r_0) p(r_1|r_0) \delta(r_{01} - (r_1 - r_0)) \quad (6)$$

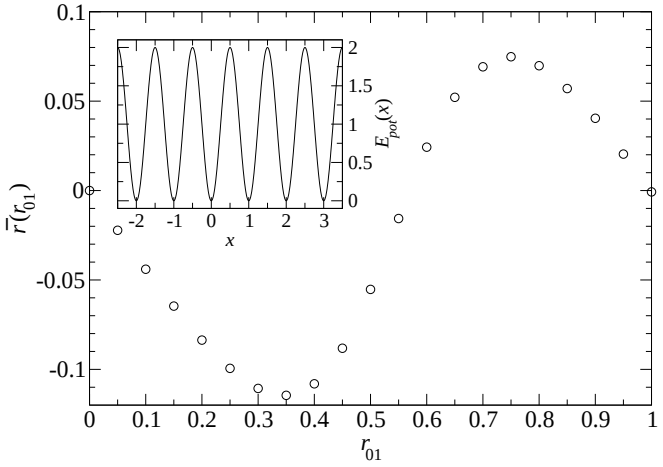

Figure 2: $\bar{r}(r_{01})$ as obtained from Monte Carlo simulations of the simple periodic cos-potential. The potential is shown in the inset.

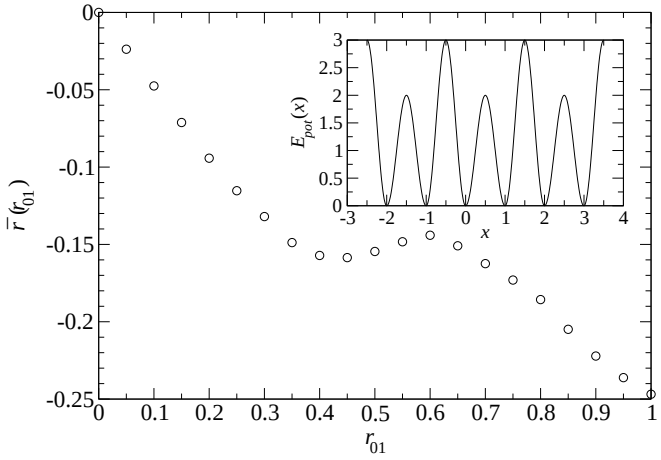

Figure 3: $\bar{r}(r_{01})$ as obtained from Monte Carlo simulations of a periodic potential with alternating barriers. The potential is shown in the inset.

where $p_0(r_0)$ denotes the equilibrium distribution and $p(r_1|r_0)$ is the probability to move from r_0 to r_1 during time t_{01}. For large t_{01} the latter term is identical to the equilibrium distribution, i.e. $p_0(r_1)$. The resulting gaussian integral can be easily solved. Here we are particularly interested in the first moment $\langle r_1 \rangle$ of $p_1(r_1)$. One obtains

$$\langle r_1 \rangle = (1/2) r_{01}. \tag{7}$$

For long t_{12} the system acquires the average $\langle r_2 \rangle = 0$, yielding

$$\bar{r}(r_{01}) = \langle r_2 \rangle - \langle r_1 \rangle = -(1/2) r_{01}. \tag{8}$$

Thus the back-dragging effect in the second time interval is proportional to the distance moved in the first time interval.

B. Periodic potential

In the next step, we analyse a potential which involves local vibrations as well as hopping dynamics. Here we consider a periodic potential $E_{pot}(r)$ with minima at integer values of r, defined as

$$V(r) = V_0[1 - \cos(2\pi r)]. \tag{9}$$

We are interested in the stochastic dynamics of a particle. In general, one has to resort to numerical simulations to calculate $\bar{r}(r_{01})$. Here we have modelled the dynamics via standard kinetic Monte Carlo simulations at the temperature $T = 0.4 V_0$ with step sizes much smaller than the distance of two adjacent minima. The qualitative features of the result do not depend on the exact value of this temperature. We have chosen t_{01} such that on this time scale a particle leaves the initial well with a probability of approximately 50%. Furthermore we have chosen $t_{12} = 10\, t_{01}$. The result of this simulation is shown in Fig. 2. The dependence of $\bar{r}(r_{01})$ on r_{01} can be understood from simple arguments: a) For $r_{01} \ll 1$, one basically has the behavior of a harmonic oscillator. b) For $r_{01} = 0.5$, the particle has typically moved to a position close to the saddle between two wells. For infinite t_{01}, simple symmetry considerations show that $\langle r_1 \rangle$ is exactly on the saddle. Since a particle on a saddle does not experience any effective net force to any side one has $\bar{r}(0.5) = 0$. For finite t_{01}, a motion of $r_{01} = 0.5$ on average leaves the particle in the initial well [28]. Thus the function $\bar{r}(r_{01})$ has its zero for r_{01} slightly larger than 0.5. c) For r_{01} approaching 1, the particle has definitely crossed a saddle. Now the effective force points in the same direction as the initial jump direction. This results in a positive value of $\bar{r}(r_{01})$. d) For $r_{01} = 1$, one has the same result as for $r_{01} = 0$, i.e. $\bar{r}(r_{01}) = 0$.

C. Potential with alternating barriers

So far we have only discussed backwards dynamics due to intrawell dynamics. For an ion conductor one expects that dynamic forward backward correlations either result from static or from dynamic disorder. Here we briefly discuss a very simple model which contains non-trivial forward backward dynamics. It is shown in the inset of Fig. 3. Due to the alternating barrier heights a particle performs several forward and backward jumps until it can escape from the local cage. We denote the two different transition rates by Γ_1 and Γ_2 ($\Gamma_1 \gg \Gamma_2$). Our goal is to calculate $\bar{r}(r_{01} = 1)$. For very long t_{01}, i.e. $t_{01}\Gamma_2 \gg 1$ the dynamics resembles that of a random walk so that forward backward correlations should not be relevant, i.e. $\bar{r}(1) \approx 0$. Therefore we restrict ourselves to the case $t_{01}\Gamma_2 \ll 1$. The analysis is presented in Appendix A.

We obtain

$$\bar{r}(1) = -(1/2)(1-2\Gamma_2/\Gamma_1)(1-2\Gamma_2/\Gamma_1) \quad (10)$$
$$*(1-\exp(-2\Gamma_1 t_{12})) \qquad t_{01}\Gamma_1 \ll 1$$
$$\bar{r}(1) = -(1/2)(1-2\Gamma_2/\Gamma_1)(1-\Gamma_2 t_{01}) \quad (11)$$
$$*(1-\exp(-2\Gamma_1 t_{12})) \qquad t_{01}\Gamma_1 \gg 1.$$

Thus there exists a limiting value for $t_{01} \to 0$ which is reached for $t_{01} \approx 1/\Gamma_1$, i.e. the time scale of the fastest jump process. For larger values of t_{01} the back-dragging effect decreases with time; see Eq.11. $\bar{r}(1)$ approaches zero for t_{01} of the order of $1/\Gamma_2$. The physical reason is that for longer times t_{01} the particle may also cross the high barrier during the first time interval. These events strongly reduce the total back-dragging effect in the subsequent time interval. Thus the t_{01}-dependence contains valuable information about the time-scales involved in the dynamics and indicates at which time scale (here: $t_{01} \approx 1/\Gamma_2$) a simple random-walk description becomes relevant.

For $t_{12} \to 0$ one obtains $\bar{r} \to 0$. This limit is trivial since there is no dynamics during the second time interval. In contrast, for $t_{12} \to \infty$ the backjump effect is largest. Thus it is this limit which is relevant to judge the maximum backjump capabilities. The rest of the discussion for this model system deals with this case.

To show the full dependence of $\bar{r}(r_{01})$ on r_{01} we again performed Monte Carlo simulations for a potential with alternating barriers. This potential was generated from the cos-potential, discussed above, by scaling the cos-potential by a factor 1.5 in the intervals $..., [-1,0], [1,2], [3,4], ...$ The temperature was $T = 0.5V_0$. t_{01} is chosen such that the short-time limit $t_{01} < 1/\Gamma_1$ is fulfilled whereas t_{12} corresponds to the long-time limit $t_{12} \gg 1/\Gamma_2$. The transition rate is proportional to the attempt frequency in the minimum, which scales with the square root of the force constant and with the Boltzmann factor. Thus one expects $\Gamma_2/\Gamma_1 \approx \sqrt{1.5}\exp((2-3)/0.5) \approx 0.17$ which, according to Eq.10, yields $\bar{r}(1) \approx 0.22$.

The result for $\bar{r}(r_{01})$ is shown in Fig. 3. It resembles that of a periodic potential except for a systematic downward trend. Thus we have a superposition of the correlation effects of simple periodic potentials with wells and barriers and of barriers with different heights. Actually, it turns out that our estimate of $\bar{r}(1)$ agrees reasonably well with the numerical value of ca. 0.25.

D. Random trap model

Finally, we want to present a very simple model which allows one to grasp the relevant features of the second moment $v(r_{01})$. We start with an (possibly high-dimensional) array of traps with different depths. Such models have been extensively studied in the context of supercooled liquids [29, 30, 31]. Different rates Γ_i are randomly attributed to the different traps. For such a simple model the dynamics is purely diffusive. Here we are specifically interested in the ratio $V(t) \equiv v(r_{01} = 1,t)/v(r_{01} = 0,t)$ for $t_{01} = t_{12} = t$. According to our discussion in Section III $V(t)$ is a measure for the relevance of dynamic heterogeneities.

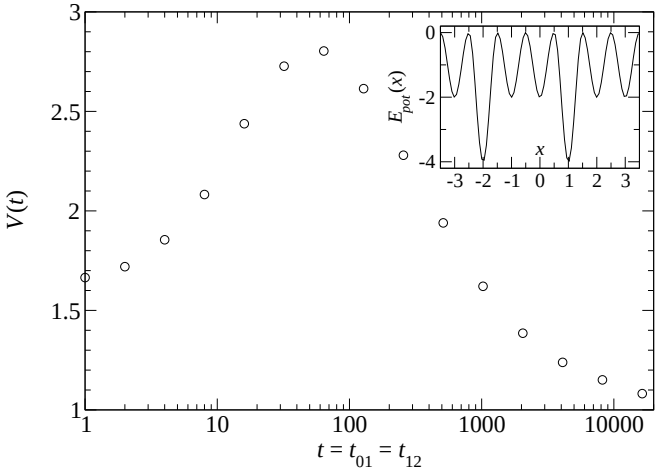

Figure 4: $V(t)$ as obtained from Monte Carlo simulations of a potential with random traps. The potential is shown in the inset.

As shown in Appendix B one can derive the relation

$$V(t \to 0) = \langle\Gamma\rangle \left\langle \frac{1}{\Gamma} \right\rangle . \quad (12)$$

Without dynamic heterogeneities it does not matter whether or not a particle moves in the first time interval such that $v(r_{01} = 1,t) = v(r_{01} = 0,t)$. In case of no dynamic heterogeneities, i.e. a single value of Γ, one trivially has $\langle\Gamma\rangle = 1/\langle 1/\Gamma\rangle$ and thus $V(t) = 1$. For a distribution of jump rates the product $\langle\Gamma\rangle\langle 1/\Gamma\rangle$ is larger than one. This can be easily rationalized for a bimodal rate distribution with rates Γ_1, Γ_2 and weights a_1, a_2, respectively. A straightforward calculation yields $V(t) = 1 + (a_1 a_2)(\Gamma_1 - \Gamma_2)^2/(\Gamma_1\Gamma_2)$ which for a bimodal distribution is strictly larger than one. For stronger dynamic heterogeneities, i.e. a broader distribution of rates Γ, $V(t)$ also increases. Thus $V(t \to 0)$ is a direct measure for dynamic heterogeneities.

In the opposite limit $t \to \infty$, a particle with $r_{01} = 0$ has by chance returned to the original position. This implies that the condition $r_{01} = 0$ no longer implies any dynamical selection of slow particles. Thus one expects $V(t \to \infty) = 1$. Whereas the detailed time-dependence of $V(t)$ depends on more details of the model like the number of neighbor traps, the limiting values are generally valid.

In order to visualize the full time-dependence, and to check our analytic expression we have performed Monte-Carlo simulations for a one-dimensional random trap model. We have chosen two escape rates, characterized by $a_1 = 0.035, a_2 = 0.965, \Gamma_1 = 0.005, \Gamma_2 = 0.1$. For this specific choice of parameters one has $\langle\Gamma\rangle\langle 1/\Gamma\rangle = 1.61$.

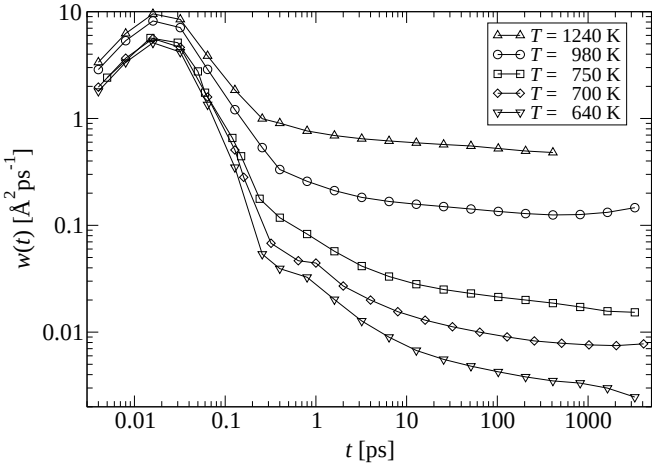

Figure 5: The derivative $w(t)$ of the mean square displacement shown for different temperatures. Note that for $t > 1ps$ the function $w(t)$ is mainly governed by long-range dynamics (see text).

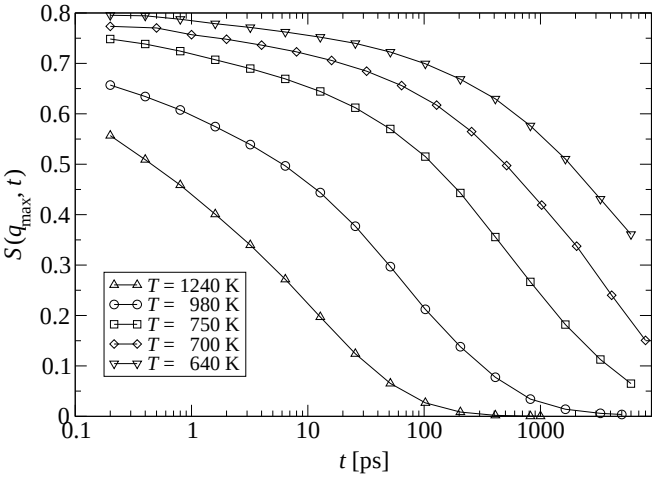

Figure 6: The incoherent scattering function $S(q_{max}, t)$ at different temperatures. The solid lines correspond to KWW-fits with $\beta = 0.45$.

The time dependence of $V(t)$ is shown in Fig. 4 as obtained via Monte Carlo simulations. For this simple model the algorithm can be implemented in a straightforward way. One observes that the theoretical short-time and long-time limits are confirmed by the numerical data. Interestingly, $V(t)$ displays a maximum. Qualitatively, this means that at the time scale of the maximum the effects of dynamic heterogeneities are most pronounced. A more detailed discussion of the time-dependence and of the maximum is beyond the scope of the present paper.

V. RESULTS

A. Previous results

It has been observed that lithium trajectories can be described as a series of local vibrations and jumps between adjacent ionic sites; see e.g. Refs.[32, 33] for similar features in previous simulations on alkali silicates. In our recent work we have shown that the van Hove self correlation function displays a strong peak for $d_0 \approx 2.6$ Å. This peak is separated by a minimum at 1.5 Å from the peak at the origin. The interpretation is straightforward. The potential energy landscape, as supplied by the network, provides lithium sites with an average distance of 2.6 Å which are separated by a saddle.

Furthermore, it turned out that the mean square displacement curves at different temperatures show time-temperature superposition. In Fig. 5 we show their derivative, i.e. $w(t)$, for the five temperatures analysed in our prior work [7]. As shown in [7] the function $w(t)$ for $t > 1ps$ is due to processes which involve long-range dynamical processes ($|\vec{r}(t) - \vec{r}(0)| \geq 1.5$ Å). Whether or not these processes can always be interpreted as jumps is currently under investigation. For $t < 1ps$ the function $w(t)$ is dominated by localized processes of the lithium ions. Since the presence of back and forth dynamics is equivalent to a decrease of $w(t)$ with time, one directly sees that at least in the case of the two lowest temperatures $T = 700$K and $T = 640$K long-range back and forth correlations are indeed important. In order to characterize the typical time scales of the long-range dynamical processes we show in Fig. 6 the incoherent scattering function $S(q_{max}, t)$ where $q_{max} = 2\pi/d_0$. It is a measure of the probability that an ion is still (or again) at the initial site after time t. All data can be consistently fitted with a KWW-function $f(t) \propto \exp(-(t/\tau)^{\beta})$ with $\beta = 0.45$.

B. Back and forth dynamics

A quantitative analysis of the back and forth dynamics is possible on the basis of the first moment $\bar{r}(r_{01})$. In Fig. 7, we have plotted this function for a fixed value of $t_{01} = 102.4$ ps and different t_{12} at $T = 750$ K. For large r_{01} the statistics of these curves becomes quite poor since only a few ions participate. This problem becomes worse for short t_{01} and/or long t_{12}. In this and the following plot we restrict ourselves to the r_{01}-regions which possess a reasonable signal-to-noise ratio as estimated from the fluctuations of the curves.

On a qualitative level the dependence on r_{01} resembles that shown in Fig. 3. For small r_{01} one recovers the harmonic behavior, as seen from the very good agreement with the broken line $\bar{r}(r_{01}) = -(1/2)r_{01}$. Furthermore the non-monotonic behavior directly reflects the presence of a saddle between adjacent lithium sites. Fig. 7 clearly reveals that the fraction of back and forth dynamics in-

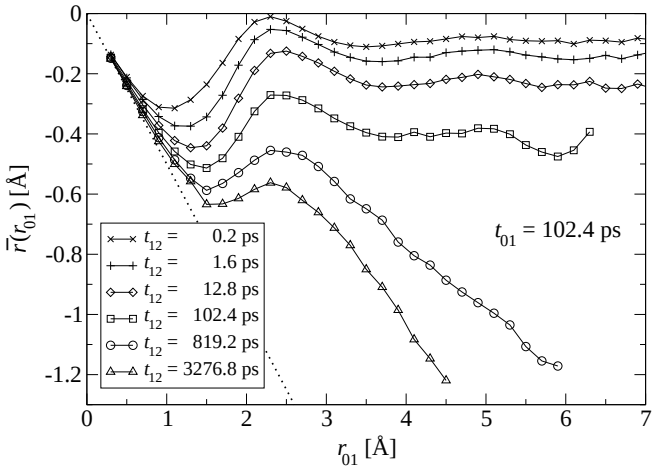

Figure 7: The first moment $\bar{r}(r_{01})$ for $t_{01} = 102.4ps$ and for different t_{12} at $T = 750$ K. The broken line corresponds to $\bar{r}(r_{01}) = -(1/2)_{01}$.

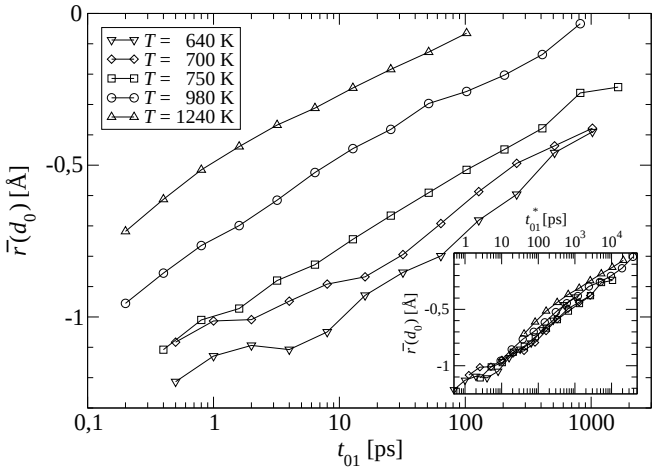

Figure 8: The first moment $\bar{r}(d_0 = 2.6\text{Å})$ in dependence of t_{01}. The value of t_{12} has been scaled for every temperature on the basis of the diffusion constant [t_{12}(T = 640 K) = 3276.8 ps]. In the inset also the values of t_{01} are scaled by the diffusion constant such that $t_{01}(T = 640K) \equiv t^*_{01}(T = 640K)$.

creases with increasing t_{12}. This is expected from our theoretical considerations; see above.

Interestingly, for the two largest values of t_{12} the function $\bar{r}(r_{01})$ decays further for $r_{01} > d_0 = 2.6$ Å. Thus back-dragging effects become stronger when jumping into the second nearest neighbor shell during t_{01}. This observation already goes beyond a scenario which is only based on back and forth correlations between adjacent lithium sites.

Of particular interest is the dependence on t_{01} as already discussed for the alternate barrier model. Since we are mainly interested in correlated back and forth dynamics between nearest-neighbor positions we focus on the value of $\bar{r}(d_0)$ which characterizes the subsequent dynamics of a particle which has jumped to the nearest neighbor distance in the first time interval. We choose a large but constant value for t_{12} (4.1 ns ps for T = 640 K) and vary t_{01}. Comparison of different temperatures is achieved by choosing the respective value of t_{12} approximately proportional to the inverse diffusion constant. This results in $t_{12} = 26ps(T = 1240K), t_{12} = 102ps(T = 980K), t_{12} = 0.8ns(T = 750K), t_{12} = 2.0ns(T = 700K), t_{12} = 4.1ns(T = 640K)$. The data are shown in Fig. 8. Obviously, for longer times t_{01} the back-dragging effect becomes much smaller. This agrees with the theoretical considerations, discussed for the alternate barrier model. The limiting value $\bar{r}(d_0) = -1.3$ Å is only approximately reached for the lowest temperature $T = 640$ K. Interestingly, the dependence on t_{01} is very gradual and extends over several decades of time. This shows that there exists a broad distribution of barriers experienced by the lithium ions.

For a fixed value of t_{01} the relevance of correlated back and forth dynamics increases with decreasing temperature. From our previous discussion the short-time limit of $t_{01} \approx 1$ ps is related to the dispersion according to Eq. 5. Since only for $t_{01} > 1$ ps long-range processes become relevant one should choose $t_{01} = 1$ ps as the short-time limit in Eq.5. Checking it, e.g. for $T = 750$K, one obtains $\bar{r}(d_0) = -1$ Å which according to Eq. 5 corresponds to $w(t \to \infty)/w(1ps) = 0.23$. This agrees with the measured value of ca. 0.2 (see Fig. 5). Note that Eq.5 is based on a strict hopping picture. Therefore one would not expect an exact agreement between both values. In any event, since only for $T \leq 750$ K $\bar{r}(d_0)$ comes close to the limiting value of -1.3 Å the back-dragging effect and, equivalently, the dispersion in the mean square displacement are relevant only in this low-temperature range.

In the inset of Fig. 8 the individual curves are scaled with the scaling factor $D(T)/D(T = 640K)$, thereby introducing the scaled time t^*_{01}. Within the statistical noise one can see a decent superposition, in particular for the three lowest temperatures. Thus one observes a time-temperature superposition also for this rather involved quantity of correlated back and forth dynamics.

C. Dynamic heterogeneities

Finally we present results for the second moment $v(r_{01})$. In Fig. 9 we have plotted $v(r_{01})$ for $T = 750$ K and different values for $t_{01} = t_{12}$. One can clearly distinguish two regimes which are approximately separated by 2 Å. For $r_{01} \ll 2$Å, the second moment $v(r_{01})$ is significantly smaller than for values $r_{01} \geq 2$ Å. As discussed above this is a clear signature of dynamic heterogeneities. After a jump of 2 Å an ion has basically achieved to cross the saddle and is already part of the adjacent ionic site. This means that a particle which has crossed the local saddle during the first time interval is much faster during the subsequent time interval. Starting from $r_{01} = d_0$ the second moment $v(r_{01})$ further increases with increas-

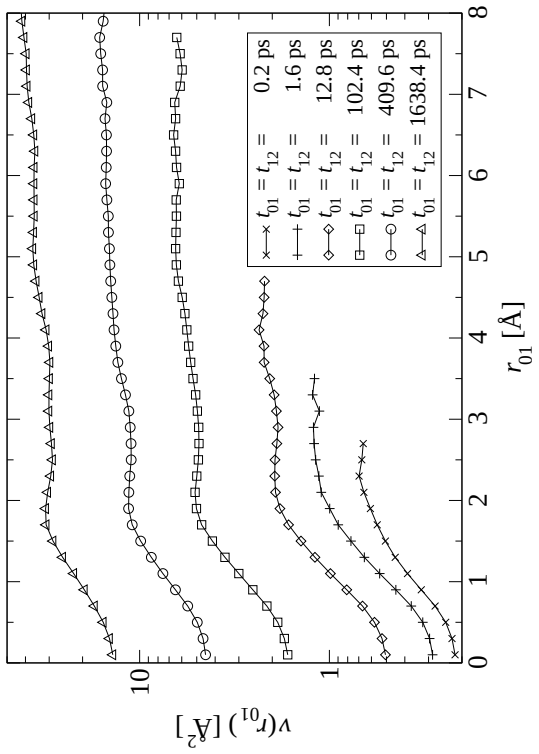

Figure 9: $v(r_{01})$ at $T = 750$K for different choices of $t_{01} = t_{12}$.

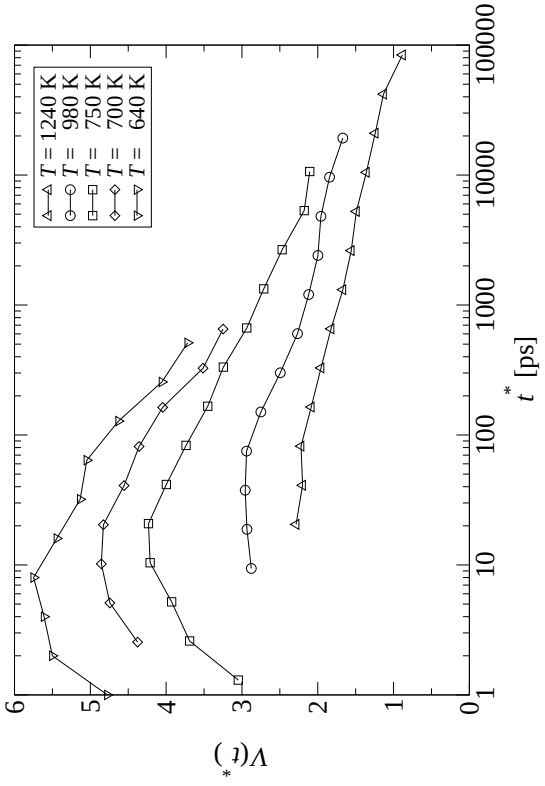

Figure 10: $V(t^*) = v(d_0)/v(0)$ at different temperatures using scaled times.

ing r_{01}. This further increase, however, is much weaker. This observation would be compatible with only minor spatial correlations among ionic sites of similar mobility. In particular, it would contradict the scenario of compact regions of ionic sites each with a different ionic mobility. In this case, a particle which has jumped twice would, on average, belong to a faster region than particles which only jumped once during the first time interval. This difference would show up in the mean square displacement during the second time interval since particles in the faster region would, on average, also jump further in the second time interval. This would lead to a strong increase of $v(r_{01})$ beyond the nearest neighbor distance d_0.

In order to study the temperature dependence and the time-dependence in greater detail we have calculated $V(t) \equiv v(d_0)/v(0)$ in dependence of $t = t_{01} = t_{12}$ and for different temperatures. $V(t)$ is a direct measure for the degree of dynamic heterogeneity on the length scale of the nearest-neighbor distance. In order to compare the different temperatures we have again scaled all times by the ratio $D(T)/D(T = 640K)$. The results are shown in Fig. 10. One can clearly see that the degree of heterogeneity changes with temperature. The lower the temperature the stronger the dynamic heterogeneity. Thus on the level of dynamic heterogeneities the time-temperature superposition principle does not hold. For the lowest temperature $V(t)$ is approximately 5.5 at the maximum. This number directly implies that the mean square displacement of a particle (corrected for possible backwards correlations) is 5.5 times larger in the second time interval if it has performed a jump in the first time interval as compared to particles which are still at the initial site after t_{01}.

VI. DISCUSSION

In this paper we have shown how analysis of three-time correlations can be used to get model-free information about the nature of the complex ion dynamics. The characteristics of back and forth dynamics is reflected by the first moment of the three-time conditional probability function, the dynamic heterogeneities by the second moment. The main results are: (i) the long-range backward correlations beyond the nearest neighbor position, (ii) the gradual decrease of backward correlations with

increasing t_{01}, (iii) the time-temperature superposition principle for correlated back and forth dynamics, (iv) the significant dynamic heterogeneities at low temperatures, and (v) the lack of time-temperature superposition for the dynamic heterogeneities. In what follows we discuss these results in more detail.

For ion conductors at low temperatures the basically immobile network serves as a pseudo-external field for the lithium ions. Therefore it has been attempted to model the lithium dynamics by simple lattice models like the random barrier or the random energy model [2, 34]. Also in these models the long-range backward correlations are present. Only in simple models like the alternate barrier model, discussed in this paper, back and forth jumps are restricted to the nearest neighbor position. The reason for these long-range backward correlations is quite intuitive: the ions look for paths which can can be accessed rather easily. In particular at low temperatures these paths can be rather extended. Only for long times the ions manage to escape such a local path. This picture is consistent with the percolation approach which has been successfully applied to describe the dynamics in the random barrier and the random energy model [2, 35].

It may be interesting to compare this scenario with that of supercooled liquids. There all particles move on the same time scale. No pseudo-external fields are present. The complexity of the dynamics is due to the necessity of cooperative dynamics of the strongly interacting particles. A simple picture is to view a particle localized in the cage of the adjacent particles. The relevant relaxation process is to escape this local cage and afterwards being trapped in a new cage. In this case the first moment $\bar{r}(r_{01})$ is constant for values of r_{01} larger than the typical nearest-neighbor distance [21]. This is due to the fact that after leaving the initial cage no significant memory to that cage is left. The r_{01}-dependence of $\bar{r}(r_{01})$ for $r_{01} > d_0$ shows that this simple cage picture cannot be used for the ionic dynamics. A possible explanation for this effect is the relevance of the static disordered energy landscape in ion conductors which leads to a dramatic reduction of multi-particle correlations [7] such that cages, formed by adjacent ions, are less relevant. Alternatively, one might argue that the presence of long-range Coulomb interaction gives rise to long-range backward correlations. This aspect still has to be clarified.

In the alternate barrier model the dependence of $\bar{r}(d_0)$ on t_{01} reflects the values of the lowest and highest relevant barriers present in the system. On the time scale for which the highest relevant barrier is crossed no back and forth dynamics should be visible. Indeed, we see in Fig. 8, e.g. for T = 750 K, that the back and forth dynamics becomes small for t_{01} of the order of 1 ns. The relaxation time, i.e. the decay time of $S(q_{max}, t)$, is of the same order. Within the alternate barrier model one expects that for t_{01} somewhat smaller than $1/\Gamma_2$ but still larger than $1/\Gamma_1$ one expects a linear dependence of $\bar{r}(d_0)$ on t_{01} in marked contrast to the numerical results. This clearly shows that in contrast to the alternate barrier model the lithium metasilicate system is characterized by a broad distribution of relevant barriers. Furthermore no short-time limit is visible in Fig. 8 but $\bar{r}(d_0)$ decreases also for the shortest times which could be analysed. This indicates the presence of transitions with very small saddles or, possibly, broad anharmonic potentials which are already relevant on the time scale of a few hundred femtoseconds.

The alternate barrier model differs from our lithium metasilicate system also in another respect. For the alternate barrier model the typical jump time is of the order of $1/\Gamma_1$. One can show that (i) the decay of $w(t)$ is strongest for exactly this time scale and (ii) $S(q = 2\pi, t \approx 1/\Gamma_1)$ is already significantly smaller than unity. For the lithium metasilicate system at, e.g., $T = 640$ K the decay of $w(t)$ (due to long-range processes; see above) is strongest in the ps range whereas $S(q, t)$ is still close to the short-time plateau value. This discrepancy could be alleviated by introducing an additional variation of site energies. This would shift the decay of $S(q, t)$ to times of the order of $1/\Gamma_2$. On a qualitative level this would imply that the short-time dynamics occurs in asymmetric double-well potentials. It remains an important question whether the same scenario also holds in lithium metasilicate, i.e. whether fast back and forth jumps in strongly asymmetric double-well potentials are present. Another scenario to rationalize the above-mentioned discrepancy will be presented further below.

In Ref. [9] it has been reported that for sodium silicate at T = 2000 K no backward correlations were observed. This is compatible with the experimental data for sodium silicate where the dispersion disappears for T $\approx$ 1000 K. [5]. For the present system the dispersion disappears around a similar temperature. This shows up in a very little time-dependence of $w(t)$ at 980 K in Fig.5 beyond 1 ps. Nevertheless, even these weak backward correlations are directly visible by analysis of the three-time correlations in Fig.8. As discussed below these backward correlations may be due to a small number of ions. Thus a less detailed analysis may oversee these backward correlations.

The approximate time-temperature superposition principle as seen in Fig. 8 implies that the back-dragging effect remains the same if analysed on appropriately adjusted time scales. Note that this statement goes beyond the previous result that the mean square displacement displays time-temperature superposition. As discussed above the latter observable is only related to the $t_{01} \to 0$ limit of $\bar{r}(r_{01})$. The time-temperature superposition in Fig. 8 may be used to discriminate between different models of ion dynamics.

The significant heterogeneities, as characterized by the second moment, is compatible with the above-mentioned broad distribution of relevant barriers. Actually, such a distribution complicates the interpretation of the dispersion $w(t \to \infty)/w(0)$ in terms of correlated back and forth dynamics. This is exemplified for the simple case of

two (temporarily distinct) ionic species with jump rates $\Gamma_1 \gg \Gamma_2$ which are present with probabilities p_1 and p_2, respectively. If we have in mind a log-gauss distribution of rates one should choose $p_1 > p_2$. Generalizing Eq.5 we get

$$\frac{w(t\to\infty)}{w(t\to 0)} = \frac{1}{2} + \frac{1}{d_0}\frac{p_1\Gamma_1\bar{r}^1 + p_2\Gamma_2\bar{r}^2}{p_1\Gamma_1 + p_2\Gamma_2} \qquad (13)$$

The terms $\Gamma_i p_i$ imply that during the short time interval t_{01} the probability of a particle of species i to perform a hop is proportional to the rate and its occurrence probability. In the limit, discussed above, and under the additional assumption that $|\bar{r}^1|$ is not much smaller or even larger than $|\bar{r}^2|$, this can be approximated by

$$\frac{w(t\to\infty)}{w(t\to 0)} \approx \frac{1}{2} + \frac{\bar{r}^1}{d_0}. \qquad (14)$$

This result shows that the dispersion is to a large degree determined by the backjump properties of the *fast* species. Thus in case of significant dynamic heterogeneities one has to be careful to relate the dispersion of the mean square displacement to the average backjump properties (here: $(p_1\bar{r}^1 + p_2\bar{r}^2)/d_0$) of the ions.

This observation allows one to envisage another explanation of the very different time scales where the decay of $w(t)$ is maximum (ps regime) and where the incoherent scattering function $S(q_{max}, t)$ decays (ns regime); see above. A few fast ions with significant back- and forth correlations can dominate the time-dependence of $w(t)$ but hardly contribute to the decay of the incoherent scattering function. Actually, for the random energy model we have observed that the back and forth correlations are strongest for the fast particles such that this effect is indeed present there. Whether it is this scenario or the above-discussed presence of energetic disorder, which dominates the different time dependence of $w(t)$ and $S(q_{max}, t)$ for lithium metasilicate, awaits further clarification.

We have shown that the degree of heterogeneity depends on temperature. In contrast, the incoherent scattering function $S(q_{max}, t)$ fulfills the time-temperature superposition principle. Actually, the same observations have been made for glass-forming liquids [11]. For these systems the non-exponentiality of $S(q_{max}, t)$ mainly reflects the broad distribution of relaxation times. Thus naively one would expect a lower value of the KWW-exponent β with increasing degree of heterogeneity. It still has to be shown why at least in the temperature range, accessible to simulations, this is not the case.

It may be interesting to compare our approach with that of Habasaki and Hiwatari [10]. For the same system at T = 700 K they determined during 1 ns the distribution of square displacements of all particles. They observed a large variance, thus indicating some distribution of relaxation times. On a qualitative level this result is compatible with the results reported above. One advantage of the present approach is that via study of the r_{01}-dependence also information about length scales are available. Furthermore, the value of $V(t \to 0)$ has a direct interpretation in terms of local rate distributions.

Having identified several properties of the complex ion dynamics in quantitative terms one would like to relate them to more microscopic properties like the distribution of oxygens around the lithium ions and to see whether mainly the interaction among the different ions or the interaction with the basically static network gives rise to the observations reported in this work.

Acknowledgments

In this work we have profited from helpful discussions with C. Cramer, K. Funke, J. Habasaki, H. Lammert, and B. Roling.

Appendix A:

Calculation of $\bar{r}(r_{01} = 1)$ proceeds in two steps. First we calculate the probability that a particle has moved by one unit to the right during some time t_{01}. Since we have two non-equivalent sites we have to calculate, on the one hand, the transition probability q_{eo} (eo stands for even-odd) from $r = 0$ to $r = 1$ and, on the other hand, the transition probability q_{oe} from $r = 1$ to $r = 2$. In the second step we calculate the average motion Δr_e (starting, e.g., from $r = 2$) and Δr_o (starting, e.g., from $r = 1$) during the second time interval. One expects $\Delta r_e > 0$ and $\Delta r_o < 0$ and for reasons of symmetry $\Delta r_e = -\Delta r_o$ which we abbreviate as Δr. With this information we can finally calculate

$$\bar{r}(1) = \frac{\Delta r_o q_{eo} + \Delta r_e q_{oe}}{q_{eo} + q_{oe}} = -\Delta r \frac{q_{eo} - q_{oe}}{q_{eo} + q_{oe}}. \qquad (A1)$$

For the calculation of q_{eo} and q_{oe} we take into account that in the limit $t_{01}\Gamma_2 \ll 1$ multiple transitions over the higher barrier can be neglected. We start with a particle either at $r = 0$ or $r = 1$ and we are interested in the probability to be at $r = 1$ or $r = 2$ after time t_{01}, respectively. Neglecting those terms, which are only relevant in case that a particle has crossed a high barrier at least twice, we end up with the following system of rate equations for the site populations p_i

$$(d/dt)p_0 = -(\Gamma_1 + \Gamma_2)p_0 + \Gamma_1 p_1 \qquad (A2)$$
$$(d/dt)p_1 = -(\Gamma_1 + \Gamma_2)p_1 + \Gamma_1 p_0 \qquad (A3)$$
$$(d/dt)p_2 = -\Gamma_1 p_2 + \Gamma_1 p_3 + \Gamma_2 p_1 \qquad (A4)$$
$$(d/dt)p_3 = -\Gamma_1 p_3 + \Gamma_1 p_2. \qquad (A5)$$

This set of differential equations can be directly solved. q_{eo} can be identified as p_1 with initial condition $r = 0$ and q_{oe} as p_2 with initial condition $r = 1$. One obtains after a short calculation

$$q_{eo} = (1/2)(1 - \Gamma_2 t_{01})(1 - \exp(-2\Gamma_1 t_{01})) \qquad (A6)$$

and

$$q_{oe} = \frac{\Gamma_2}{4\Gamma_1}[1 - \exp(-2\Gamma_1 t_{01}) + \Gamma_1 t_{01}(1 + \exp(-2\Gamma_1 t_{01})]. \tag{A7}$$

Thus we finally get (using again $\Gamma_1 \gg \Gamma_2$)

$$\frac{q_{eo} - q_{oe}}{q_{eo} + q_{oe}} = 1 - 2\frac{\Gamma_2}{\Gamma_1} \ (t_{01}\Gamma \ll 1) \tag{A8}$$

and

$$\frac{q_{eo} - q_{oe}}{q_{eo} + q_{oe}} = 1 - \Gamma_2 t_{01} \ (t_{01}\Gamma \gg 1). \tag{A9}$$

As a second ingredient we want to calculate Δr which is the average coordinate $\langle r \rangle$ after time t_{12} for the initial condition $r = 0$. Using the standard trick of introducing the functions

$$S_q \equiv \sum_j p_j \exp(iqj) \tag{A10}$$

and

$$T_q \equiv \sum_j (-1)^j p_j \exp(iqj) \tag{A11}$$

one can write down two linear differential equations involving T_q and S_q

$$(d/dt)S_q(t) = -(\Gamma_1 + \Gamma_2)S_q(1 - \cos q) - i(\Gamma_1 - \Gamma_2)T_q \tag{A12}$$

$$(d/dt)T_q(t) = -(\Gamma_1 + \Gamma_2)T_q(1 + \cos q) + i(\Gamma_1 - \Gamma_2)S_q \tag{A13}$$

which can be solved with standard methods after specification of the initial condition. Of interest for us is the expectation value $\langle r \rangle$ for the initial condition $r(0) = 0$. This expression can be calculated from

$$\langle r \rangle = -i \lim_{q \to 0} (d/dq) S_q. \tag{A14}$$

It turns out

$$\Delta r = (1/2)\frac{\Gamma_1 - \Gamma_2}{\Gamma_1 + \Gamma_2}(1 - \exp(-2(\Gamma_1 + \Gamma_2)t_{12})) \tag{A15}$$

which in the limit $\Gamma_1 \gg \Gamma_2$ can be rewritten as $\Delta r = (1/2)(1 - 2\Gamma_2/\Gamma_1)(1 - \exp(-2\Gamma_1 t_{12}))$.

Thus we have calculated all ingredients which are necessary for determination of $\bar{r}(1)$.

Appendix B:

Here we calculate the short-time limit of the random trap model. We always choose $t_{01} = t_{12} = t$. We define the probability that a trap has the escape rate Γ_i as p_i. In equilibrium the probability that a particle is in a trap with escape rate Γ_i is proportional to p_i/Γ_i. Then we can write

$$v(r_{01} = 1, t) = \frac{\sum_{i,j}(p_i/\Gamma_i)p_j q_i(t) r_j^2(t)}{\sum_{i,j}(p_i/\Gamma_i)p_j q_i(t)}. \tag{B1}$$

Here $q_i(t)$ denotes the probability that after time t the particle has moved by one unit, starting in a trap with escape rate Γ_i and $r_j^2(t)$ the short-time expression for the mean square displacement, starting from a trap with rate Γ_j. One simply has $q_i(t) = \Gamma_i t$ and $r_j^2(t) = \Gamma_j t$. After a short calculation one obtains

$$v(r_{01} = 1, t \to 0) = \sum_i p_i \Gamma_i \equiv \langle \Gamma \rangle. \tag{B2}$$

In analogy one obtains for the short-time expansion of $v(r_{01} = 0, t)$

$$v(r_{01} = 0, t) = \frac{\sum_{i,j}(p_i/\Gamma_i)p_j(1 - q_i(t))r_i^2(t)}{\sum_{i,j}(p_i/\Gamma_i)p_j(1 - q_i(t))} = \frac{1}{\langle 1/\Gamma \rangle}. \tag{B3}$$

Thus one obtains

$$\frac{v(r_{01} = 1, t)}{v(r_{01} = 0, t)} = \langle \Gamma \rangle \langle 1/\Gamma \rangle. \tag{B4}$$

[1] K. Funke, R.D. Banhatti, S. Brückner, C. Cramer, C. Krieger, A. Mandanici, C. Martiny, I. Ross, Phys. Chem. Chem. Phys. (to be published).

[2] J. C. Dyre and T. B. Schroder, Rev. Mod. Phys. **72**, 873 (2000).

[3] B. Roling, C. Martiny, and K. Funke, J. Non-Cryst. Solids**249**, 201 (1999).

[4] B. Roling, C. Martiny and S. Brückner, Phys. Rev. B **63**, 214203 (2000).

[5] T. Wong, C.A. Angell eds., Glass structure by spectroscopy, 1976, Marcel Dekker, New York.

[6] C. Cramer, S. Brückner, Y. Gao, K. Funke, R. Belin, G. Taillades and A. Pradel (J. Non-Cryst. Solids, in press).

[7] A. Heuer, M. Kunow, M. Vogel, R.D. Banhatti, Phys. Chem. Chem. Phys. 4, 3185 (2002).

[8] J. Reinisch, A. Heuer, Phys. Rev. B (in press).

[9] P. Jund, W. Kob, R. Jullien, Phil. Mag. B **82**, 597 (2002).

[10] J. Habasaki, Hiwatari, Phys. Rev. E **65**, 021604 (2002).

[11] B. Doliwa, A. Heuer, J. Phys. C: Condens. Matter 11, A277-A283 (1999).

[12] P. Jund, W. Kob, and R. Jullien, Phys. Rev. B. **64**, 134303 (2001).

[13] J. Horbach, W. Kob, K. Binder, Phys. Rev. Lett. **88** ,125502 (2002).

[14] C.A. Angell, Solid State Ionics **105**, 15 (1998).

[15] W. Götze and L. Sjögren, Rep. Prog. Phys. **55**, 241

(1992).
[16] K. Schmidt-Rohr and H.W. Spiess, Phys. Rev. Lett. **66**, 3020 (1991).
[17] A. Heuer, M. Wilhelm, H. Zimmermann, and H.W. Spiess, Phys. Rev. Lett. **75**, 2851 (1995).
[18] R. Boehmer, G. Hinze, G. Diezemann, B. Geil, and H. Sillescu, Europhys. Lett. **36**, 55 (1996).
[19] M.T. Cicerone and M.D. Ediger, J. Chem. Phys. **103**, 5684 (1995).
[20] A. Heuer and K. Okun, J. Chem. Phys. **106**, 6176 (1997).
[21] B. Doliwa and A. Heuer, Phys. Rev. Lett. **80**, 4915 (1998).
[22] J. Qian, R. Hentschke, and A. Heuer, J. Chem. Phys. **110**, 4514 (1999).
[23] M. Vogel, M. Brinkmann, H. Eckert, A. Heuer, Phys. Chem. Chem. Phys. (in press).
[24] J. Habasaki, Molecul. Phys. **70**(3), 513 (1990).
[25] J. Habasaki and I. Okada, Molecular Simulation **9**(5), 319 (1992).
[26] R.D. Banhatti and A. Heuer, Phys. Chem. Chem. Phys. **3** 5104 (2001).
[27] K. Refson, Computer Physics Communications **126** , 310 (2000).
[28] One can imagine that for very short t_{01} the only chance to move $r_{01} = 0.5$ is to start at -0.5 and roll down to the minimum, i.e. $r_1 = 0$.
[29] C. Monthus and J.P. Bouchaud, J. Phys. A - Math. Gen. **29**, 3847 (1996).
[30] T. Odagaki, Phys. Rev. Lett.**75**, 3701 (1995).
[31] B. Doliwa, A. Heuer, cond-mat 0205283.
[32] M.A. Manalang, D.B. Bergstrom, D.E. Kramer, J. Kieffer, J. Non-Cryst. Solids **169**, 72 (1994).
[33] W. Smith, G.N. Greaves, and M.J. Gillan, J. Chem. Phys. **103**, 1995 (1995).
[34] S.D. Baranovskii, H. Cordes, J. Chem. Phys. **111**, 7546 (1999).
[35] B.I. Shklovskii, A.L. Efros, *Electronic Properties of Doped Semiconductors* (Springer, Heidelberg 1984).